NANO LETTERS

2009
Vol. 9, No. 12
4352-4358

Nanoporous Pt−Co Alloy Nanowires: Fabrication, Characterization, and Electrocatalytic Properties

Lifeng Liu,* Eckhard Pippel, Roland Scholz, and Ulrich Gösele*

Max Planck Institute of Microstructure Physics, Weinberg 2, D06120 Halle, Germany

Received August 11, 2009; Revised Manuscript Received September 25, 2009

ABSTRACT

Nanoporous Pt−Co alloy nanowires were synthesized by electrodeposition of Co-rich Pt_1Co_{99} alloy into anodic aluminum oxide (AAO) membranes, followed by a dealloying treatment in a mild acidic medium. These nanowires consist of porous skeletons with tiny pores of 1−5 nm and crystalline ligaments of 2−8 nm. Morphological and compositional evolutions of the porous Pt−Co nanowires upon dealloying were investigated, and their formation mechanism is discussed. The nanoporous Pt−Co alloy nanowires are found to exhibit distinctly enhanced electrocatalytic activities toward methanol oxidation as compared to the current state-of-the-art Pt/C and PtCo/C catalysts, thus showing substantial promise as efficient anode electrocatalysts in direct methanol fuel cells.

Nanoporous metallic structures have recently attracted increasing attention because they are promising for a broad range of applications such as catalysis,[1−6] sensing,[7] surface-enhanced Raman scattering,[8] fuel cells,[9] and actuation.[10,11] Several methods have been developed to fabricate porous metallic nanostructures including liquid crystal template synthesis,[12,13] hydrothermal growth,[14−16] and chemical/electrochemical dealloying from a binary or multicomponent alloy.[1,2,5,6,17−26] Among these methods, dealloying has been widely used because it is known to be a simple and effective way for achieving well-defined three-dimensional bicontinuous nanoporous structures. As a terminology of corrosion science, dealloying refers to chemically/electrochemically selective dissolution of a less noble metal component(s) from an alloy. It can be viewed as a phase separation process (spinodal decomposition) at the solid-electrolyte interface, where the less noble metal atoms are dissolved away while the more noble metal atoms are chemically driven to aggregate into interconnected clusters, thus resulting in the formation of a porous skeleton of the more noble metal component.[17−19]

To date, nanoporous gold (NPG) is the most extensively studied porous metallic nanostructure due to its simplicity in preparation and its improved catalytic properties as compared to bulk gold. Other nanoporous metals such as Pt,[6,13,23,27] Pd,[5] Ag,[28] Ni,[29] and Cu[30] were also reported but have remained rarely explored in any detail. For catalytic applications, a bimetallic nanoporous structure would be preferable because it is well-known that bimetallic catalysts can not only reduce the loadings of the precious metal, but also distinctly improve its catalytic performance. Although the commonly accepted model for dealloying does not exclude the formation of nanoporous alloys,[17−19] most dealloyed nanoporous structures reported so far are only composed of a pure noble metal or contain a tiny amount of less noble metal as residue.[5] Snyder et al. reported the first bimetallic nanoporous structure, which was fabricated by dealloying a Ag-rich Au−Ag "precursor" alloy in a neutral solution.[22] More recently, Xu et al. also described a bimetallic mesoporous structure that was prepared by dealloying a Cu−Al alloy and a subsequent galvanic-replacement reaction between the resulting nanoporous copper and Pt (or Pd) precursors.[31]

Here, we report the formation of nanoporous Pt−Co nanowires with controllable morphologies and compositions by dealloying electrodeposited Pt_1Co_{99} nanowires in the presence of porous anodic aluminum oxide (AAO) membrane in a mild acidic medium. We demonstrate that both the morphology and composition of the dealloyed porous Pt−Co nanowires can be controlled by simply adjusting the dealloying time. Furthermore, we prove that these porous nanowires possess markedly enhanced electrocatalytic activities toward the methanol oxidation reaction (MOR) in comparison to state-of-the-art Pt/C and PtCo/C catalysts and may therefore serve as efficient anode catalysts in direct methanol fuel cells (DMFCs).

The fabrication procedure of the nanoporous Pt−Co alloy nanowires is schematically illustrated in Figure 1a−c. First, continuous and dense Pt−Co "precursor" nanowires were electrodeposited into a porous AAO membrane. The elec-

* To whom correspondence should be addressed. E-mail: (L.L.) liulif@mpi-halle.de; (U.G.) goesele@mpi-halle.de.

10.1021/nl902619q CCC: $40.75
Published on Web 10/20/2009

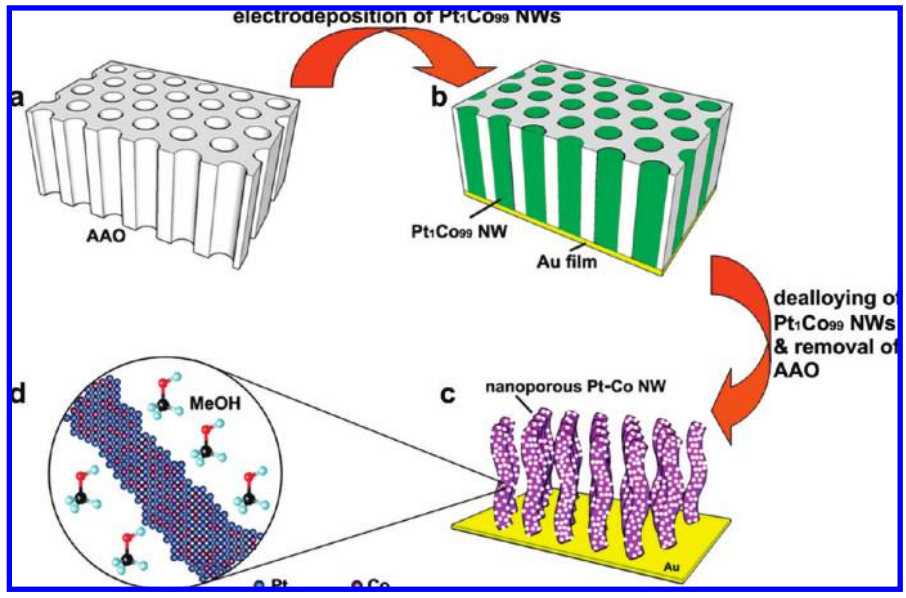

Figure 1. (a−c) Schematic illustration of the fabrication process of nanoporous Pt−Co alloy nanowires; (d) enlarged schematic of the core−shell like structure of the ligaments.

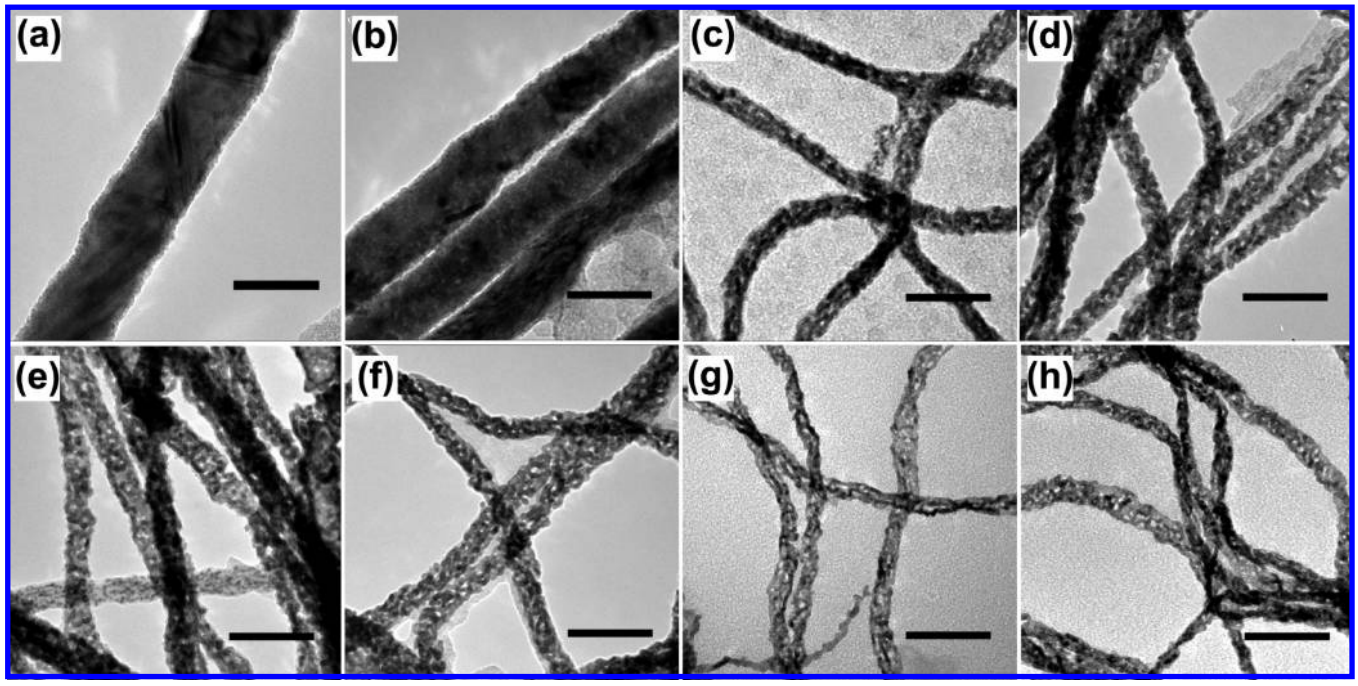

Figure 2. TEM micrographs of nanoporous Pt−Co alloy nanowires dealloyed from Pt_1Co_{99} nanowires for different dealloying times. (a) 0 min; (b) 5 min; (c) 10 min; (d) 30 min; (e) 2 h; (f) 5 h; (g) 15 h; and (h) 5 days. The dealloying was carried out in 10 wt % H_3PO_4 at 45 °C. The scale bars in (a,b) and (c−h) are 30 and 50 nm, respectively.

trodeposition was carried out under a condition that favors the reduction of Co^{2+} in the electrolyte (−1.0 V vs Ag/AgCl, see Supporting Information for details), so that only a small amount of Pt (1 at % or even less) was incorporated into the nanowires. The deposited Pt_1Co_{99} nanowires were then used as starting materials for a subsequent dealloying treatment in 10 wt % H_3PO_4 solution at 45 °C, during which most cobalt atoms were selectively dissolved and porosity evolved in the nanowires. The AAO membrane was also partly or completely removed depending on the dealloying time. According to the dealloying model,[18,19] thus-obtained nanoporous Pt−Co nanowires may have a Pt-enriched outer surface (Figure 1d). It is expected that any surface Co atoms, if existing, would be dissolved away by the acid.

Figure 2 shows the morphological evolution of Pt_1Co_{99} nanowires upon dealloying. The average diameter of as-deposited Pt_1Co_{99} nanowires is around 28 nm, consistent with the pore diameter of the AAO membranes used (produced in H_2SO_4). After 5 min dealloying in 10 wt % H_3PO_4, the wire diameter shrank to about 20 nm, and the wire surface turned to be rough, as displayed in Figure 2b. There were no visible nanopores inside the nanowires, implying that

probably only surface Co atoms were leached. As the dealloying time was extended to 10 min, the morphology of the nanowires changed distinctly. The wire diameter was reduced to 14 nm, and tiny nanopores started to evolve within the nanowires (Figure 2c), which indicates that dealloying occurred in the whole volume of the nanowires. The diameter shrinkage upon dealloying had also been observed in NPG nanowires before[7,24] and can be ascribed to plastic deformations by homogeneous slip in small ligaments or by climb of lattice dislocations during the dealloying process. Further extension of the dealloying time resulted in the appearance of a high density of nanopores along the entire nanowires, as illustrated in Figure 2d−f. The pore size varied from less than 1 to 5 nm, and the ligament width ranged from 2 to 8 nm. In addition, it was also found that the morphology of porous nanowires dealloyed for 5 h did not change much, suggesting that the porous nanowires were stable due to the protection of Pt atoms on their surfaces. However, when the dealloying time was further increased, the ligaments turned to be thinner and the pore density also slightly increased (Figure 2g,h). This may be related to the fact that some subsurface Co atoms were exposed to the acid because of the surface diffusion of Pt atoms in the acid so that they were leached away. Nevertheless, it was observed that the nanoporous morphology can remain in the acid used for dealloying at least 5 days. Moreover, in contrast to the case of NPG,[32] no obvious coarsening effect was found in the nanoporous Pt−Co alloy nanowires.

A notable feature of the as-prepared porous Pt−Co nanowires is their small pore size, which is only in the range of 1−5 nm. By contrast, the typical pore size of nanoporous Au or other nanoporous metals is 10−20 nm or even larger.[17,30,32,33] The formation of the tiny pores in Pt−Co nanowires is believed to be associated with the relatively slower surface diffusion rate of Pt with respect to Au, which makes Pt atoms prefer to sit at kink and step edge sites during dealloying.[19,21] This result is consistent with those reported previously by other authors,[21,23] indicating that the small pore size may be the common feature for dealloying-derived Pt-based nanoporous materials.

The crystallinity of nanoporous Pt−Co nanowires was examined by high resolution transmission electron microscopy (HRTEM). Figure 3 shows representative HRTEM pictures of the nanoporous Pt−Co nanowires subjected to 5 min (Figure 3b) and 15 h dealloying treatments (Figure 3d), respectively. It is clear that the nanowires remain well crystallized after dealloying though their crystallinity is not as good as that of the original electrodeposited Pt_1Co_{99} alloy nanowires (nearly single-crystalline, Supporting Information, Figure S1). This demonstrates that dealloying does not impair the crystallinity of the resulting porous structures too much, which is consistent with previous studies on bulk nanoporous metals.[20,21] The alloy nature of the porous nanowires was also confirmed by electron diffraction which revealed only a single set of diffraction rings (Figure 3c, inset).

Figure 4 shows the composition evolution of the deposited Pt_1Co_{99} nanowires with dealloying time (see Supporting Information for EDX spectra, Figure S2). With increasing dealloying time, three composition regions can be distinguished, which are denoted by pink, green and cyan, respectively. It is seen from the region I that the atomic percentages of both Pt and Co only slightly change. This could correspond to the dissolution of surface Co atoms, which is in line with the TEM observation described above (Figure 2b). Hence, region I can be identified as a "surface dealloying" region, corresponding to the initial stage of the dealloying. Region II spans the dealloying time from 10 min to 5 h. The composition altered dramatically when the Pt_1Co_{99} nanowires were subjected to dealloying for 10 min. The atomic percentage of Pt increased to 42%, while that of Co decreased down to 58%, which implied that dealloying took place in the volume of the nanowires. This is also confirmed by the greatly reduced wire diameter and the evolution of porosity, as illustrated in Figure 2c. Thereafter, the composition of the porous nanowires only varies slightly as long as the dealloying time does not exceed 5 h. This suggests that the entire outer surface of the nanoporous Pt−Co nanowires was covered by Pt atoms that blocked the further dissolution of interior Co atoms. On the other hand, as we will discuss below, the existence of the porous alumina membranes also contributed to the compositional stability in this region. In region III, it is observed that the atomic percentage of Pt further rose, accompanied by a corresponding decrease in the content of Co. As mentioned above, this is most likely related to the gradual exposure of the underlying Co atoms due to the surface diffusion of Pt atoms. Nevertheless, when the dealloying time was over 15 h, a new steady state was achieved. The composition of porous nanowires changed little with the dealloying time up to 5 days.

It was rather unexpected that well-shaped porous Pt−Co nanowires could be formed by dealloying Pt_1Co_{99} nanowires which just contained 1 at % of the noble metal. We assume that two factors played an important role. First, the presence of AAO membranes during dealloying turned out to be essential. When as-deposited Pt_1Co_{99} nanowires were first released from AAO membranes and subsequently subjected to the dealloying treatment under the same condition (i.e., 10 wt % H_3PO_4, 45 °C), no solid interconnected structures were left. It was found that the complete dissolution of AAO by 10 wt % H_3PO_4 needs more than three hours; while dealloying usually occurs at a much shorter time scale (several minutes).[19,32] This means that the dealloying actually took place in a confined environment (Supporting Information, Figure S3). In this case, the AAO membranes played a dual role. (1) The reaction between porous alumina and H_3PO_4 at the dissolution front consumes many H^+ ions, leading to a reduced dissolution rate of Co so that Pt atoms have the time and opportunity to move and passivate the nanowire surface due to their rapid surface diffusion at the alloy/electrolyte interfaces. (2) The mass transport of H_3PO_4 from the bulk solution to the dissolution front is limited by the nanochannels of AAO, and therefore the supply of H^+ ions is diffusion-limited. As mentioned above, the presence of AAO upon dealloying can be used to explain the relatively stable morphology and composition of the resulting porous nanowires in region II (Figure 4). After the appearance of

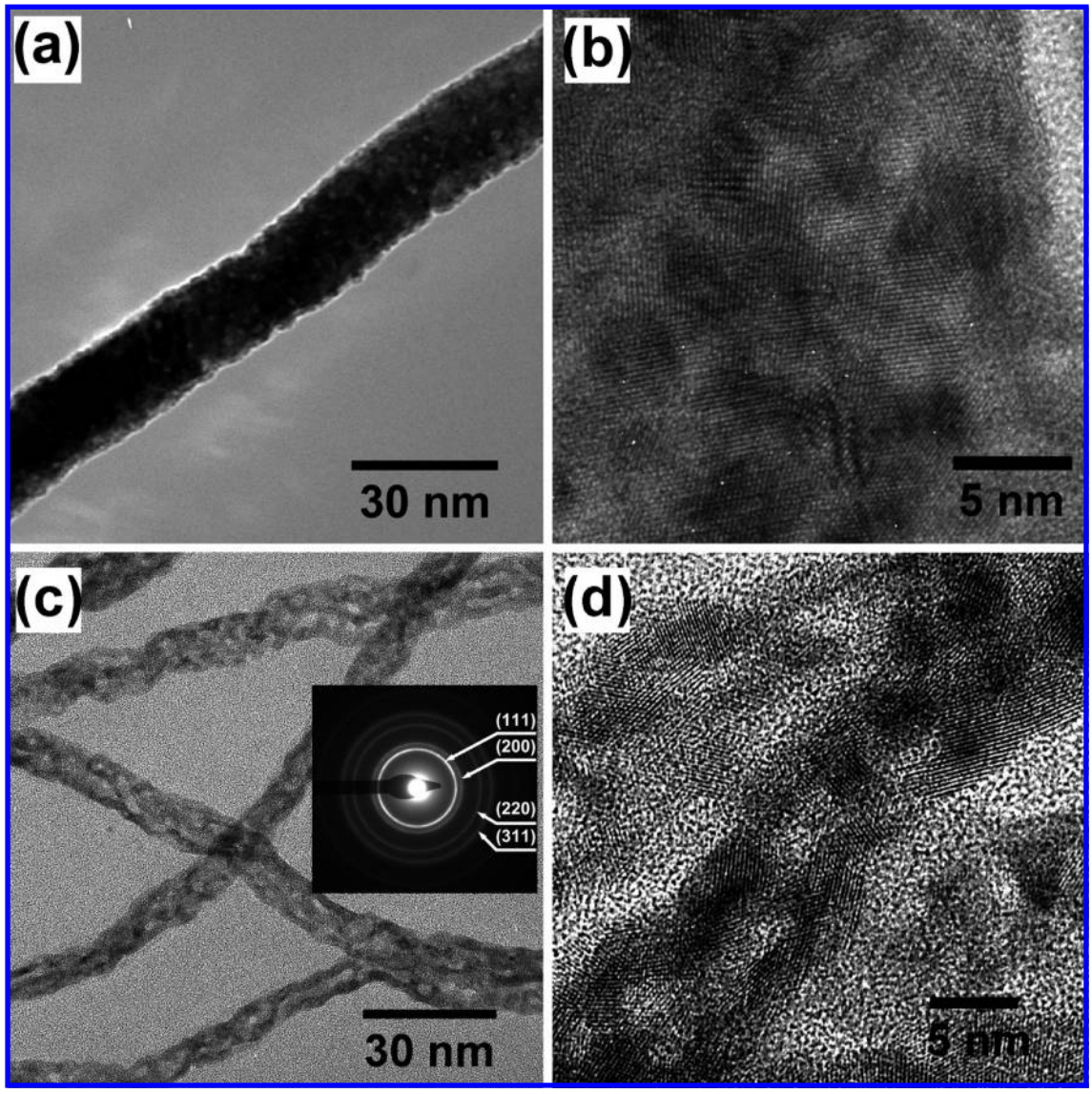

Figure 3. High-resolution TEM micrographs showing the crystalline features of as-prepared nanoporous Pt−Co alloy nanowires. (a,b) 5 min dealloying; (c,d) 15 h dealloying. The dealloying was carried out in 10 wt % H_3PO_4 at 45 °C.

porous nanostructures upon 10 min-dealloying, the acid is mainly consumed for dissolving porous alumina because the Pt-rich outer surface of porous nanowires is resistant to the etching. However, once the porous alumina is completely dissolved, the acid can freely access the porous nanowires and drive Pt atoms to diffuse at the surfaces to expose underlying Co atoms, resulting in the variation of morphology and composition. Second, the mild acidic environment is believed to be crucial for the formation of nanoporous structures. A control experiment demonstrated that if concentrated nitric acid, a commonly used etchant for dealloying, was used, there were no discernible products after dealloying even in the presence of AAO membranes. It is known that the morphology of nanoporous metals fabricated by dealloying is determined by the competition between the dissolution of the less noble component and surface diffusion of the more noble component.[34] In the case of concentrated nitric acid as etchant, the driving force for Co dissolution will be much higher so that nearly all Co atoms are quickly dissolved away before a remaining structure can be passivated by Pt atoms. In view of their quite small concentration in the alloy, the remaining Pt atoms are hard to interconnect with each other. Therefore, nanoporous structures cannot be expected in this case.

We also demonstrated that similar nanoporous Pt−Co nanowires can be achieved when AAO membranes with larger pore diameters were used in the experiments (Supporting Information, Figure S4), which illustrates that the formation of such nanoporous Pt−Co alloy nanostructures has no noticeable dependence on the pore size of the AAO membranes used in the pore size range of about 30−200 nm.

Figure 5 shows cyclic voltammograms (CVs) of several representative nanoporous Pt−Co alloy nanowire samples (30 min, 2 h, and 15 h dealloying) in Ar-saturated 0.5 M H_2SO_4 solution (see Supporting Information, Figure S5 for all CVs of the samples investigated) from which the electrochemically active surface area (ECSA, m^2/g_{Pt}) of the nanoporous Pt−Co alloy nanowires can be estimated according to the following equation

$$\mathrm{ECSA} = S_R/W_{Pt} = (Q_H/210)/W_{Pt} \quad (1)$$

where S_R represents the real surface area of the catalysts, W_{Pt} is the Pt loading (g/cm^2), Q_H stands for the total charge (μC) associated with hydrogen underpotential deposition which can be calculated by integrating the CV curve between −0.2 and 0.15 V (vs Ag/AgCl), and 210 is the charge (μC/cm$^2_{Pt}$) corresponding to the adsorption of a monolayer of hydrogen on a polycrystalline Pt surface. The calculated S_R and ECSA of the nanoporous Pt−Co nanowires as well as Pt/C (30% Pt on Vulcan XC-72, E-TEK) and PtCo/C (30% PtCo (1:1 a/o) on Vulcan XC-72, E-TEK) commercial catalysts are listed in Table 1. It is seen that the ECSA of 10 min dealloying nanoporous Pt−Co nanowires is only 19.4 m^2/g$_{Pt}$, whereas the ECSAs of 20 min, 30 min, 1 h, and 2 h dealloying samples are distinctly increased, reaching 30.4, 37.6, 34.6, and 31.1 m^2/g$_{Pt}$, respectively. For the 15 h dealloying nanoporous Pt−Co nanowires, their ECSA is further increased to 46.4 m^2/g$_{Pt}$. Nevertheless, the ECSA of all nanoporous Pt−Co nanowire samples is found to be lower than that of commercially available Pt/C or PtCo/C catalysts.

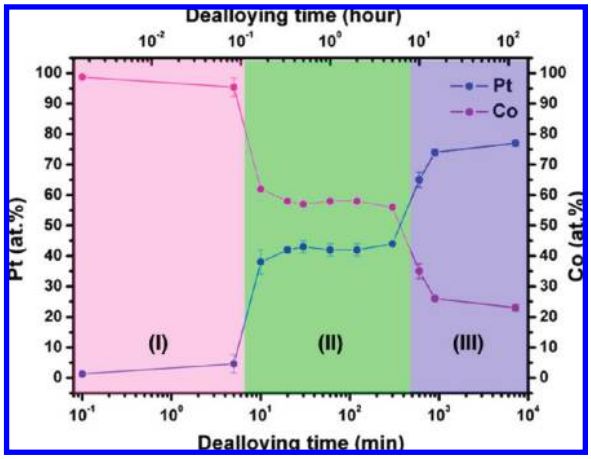

Figure 4. Composition evolution of nanoporous Pt−Co alloy nanowires versus dealloying time as measured by EDX. Region I (pink): "surface dealloying" of nanowires (see Figure 2b). Region II (green): volume dealloying within confined nanopores (see Figure 2c−f). Region III (cyan): Pt surface-diffusion-induced composition variation after the complete removal of AAO (see Figure 2g,h). For the starting Pt_1Co_{99} nanowires, for convenience the dealloying time is supposed to be 0.1 min, as the logarithm of 0 min is negative infinity and no corresponding value on the horizontal axis could be given on this type of graph.

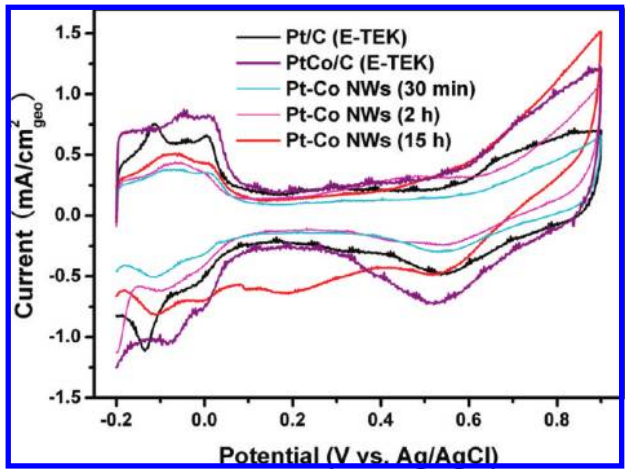

Figure 5. Cyclic voltammograms (CVs) of the nanoporous Pt−Co nanowires dealloyed for 30 min, 2 and 15 h, which were recorded in Ar-saturated 0.5 M H_2SO_4 solution at room temperature. For comparison, the CVs of commercial Pt/C (30% Pt on Vulcan XC-72, E-TEK) and PtCo/C (30% PtCo (1:1 a/o) on Vulcan XC-72, E-TEK) are also included. These CV curves are used to calculate the real surface area of the catalysts. Scan rate: 50 mV/s.

Table 1. Electrocatalytic Performance Parameters of As-Prepared Nanoporous Pt−Co Alloy Nanowires toward Methanol Oxidation[a]

sample	real surface area (cm$^2_{Pt}$/cm$^2_{geo}$)	ECSA (m^2/g$_{Pt}$)	peak current density: specific (mA/cm$^2_{Pt}$)	peak current density: mass (A/mg$_{Pt}$)	I_f/I_b
Pt/C 30 (E-TEK)	9.52	53.3	1.26	0.52	0.76
PtCo/C 30 (E-TEK)	13.16	48.7	1.70	0.83	1.32
Pt−Co NWs (10 min)	3.24	19.4	2.47	0.48	1.2
Pt−Co NWs (20 min)	5.06	30.4	2.18	0.66	1.08
Pt−Co NWs (30 min)	6.27	37.6	2.38	0.90	0.90
Pt−Co NWs (1 h)	5.76	34.6	2.61	0.90	1.11
Pt−Co NWs (2 h)	5.19	31.1	5.43	1.69	0.94
Pt−Co NWs (15 h)	7.74	46.4	5.57	2.58	0.88

[a] The real Pt surface area and electrochemically active surface area are calculated according to the voltammograms recorded in Ar-saturated 0.5 M H_2SO_4 solution at room temperature. The methanol oxidation currents were recorded in a mixed solution of 0.5 M H_2SO_4 and 1 M CH_3OH at room temperature and normalized to the real Pt surface area and the Pt mass, respectively. The working electrode area (i.e. geometrical area) is 0.196 cm^2 for Pt/C and PtCo/C catalysts and 0.636 cm^2 for nanoporous Pt−Co nanowire catalysts. Scan rate: 50 mV/s. The texts in parentheses refer to the dealloying time.

The electrocatalytic performance of the nanoporous Pt−Co alloy nanowires toward methanol oxidation was evaluated by cyclic voltammetry and chronoamperommetry (CA) in a 0.5 M H_2SO_4 aqueous solution containing 1 M CH_3OH at room temperature (Supporting Information, Figure S6). The CV and CA curves of several representative samples (30 min, 2 h, and 15 h dealloying), which are normalized by both the real Pt surface area (specific activity) and the Pt mass (mass activity), are shown in Figure 6. For comparison, the CVs and CAs of Pt/C and PtCo/C catalysts are also given. It is observed that the specific peak current density (i.e., the forward anodic peak, I_f) of Pt/C and PtCo/C catalysts are 1.26 and 1.70 mA/cm$^2_{Pt}$, and their mass peak current density are 0.52 and 0.83 A/mg$_{Pt}$, respectively. These values are comparable or higher than those reported previously[3,31,35,36] and are consistent with the well-established fact that PtCo/C catalysts have a better performance than Pt/C catalysts in terms of both specific and mass activity.[37] From Figure 6a,b, it is evident that both the specific and mass activity of nanoporous Pt−Co nanowires studied here are higher than those of Pt/C or PtCo/C catalysts. For the 15 h dealloying sample, its specific activity and mass activity are as high as 5.57 mA/cm$^2_{Pt}$ and 2.58 A/mg$_{Pt}$, respectively, which are much higher than those reported in the newly developed NPG/Pt[3,36] and NM Pt/Cu catalysts,[31] Pt nanonetworks and nanosponges[38] as well as PtCu nanoparticles,[39] but are slightly lower than those reported in the catalytically active multilayers of Pt films[40] and Pt nanosheets.[41] The mass activity of the 15 h dealloying sample (i.e., nanoporous Pt_3Co nanowires) is found to be 5 times higher than that of Pt/C. This implies that the Pt loading can be markedly reduced if

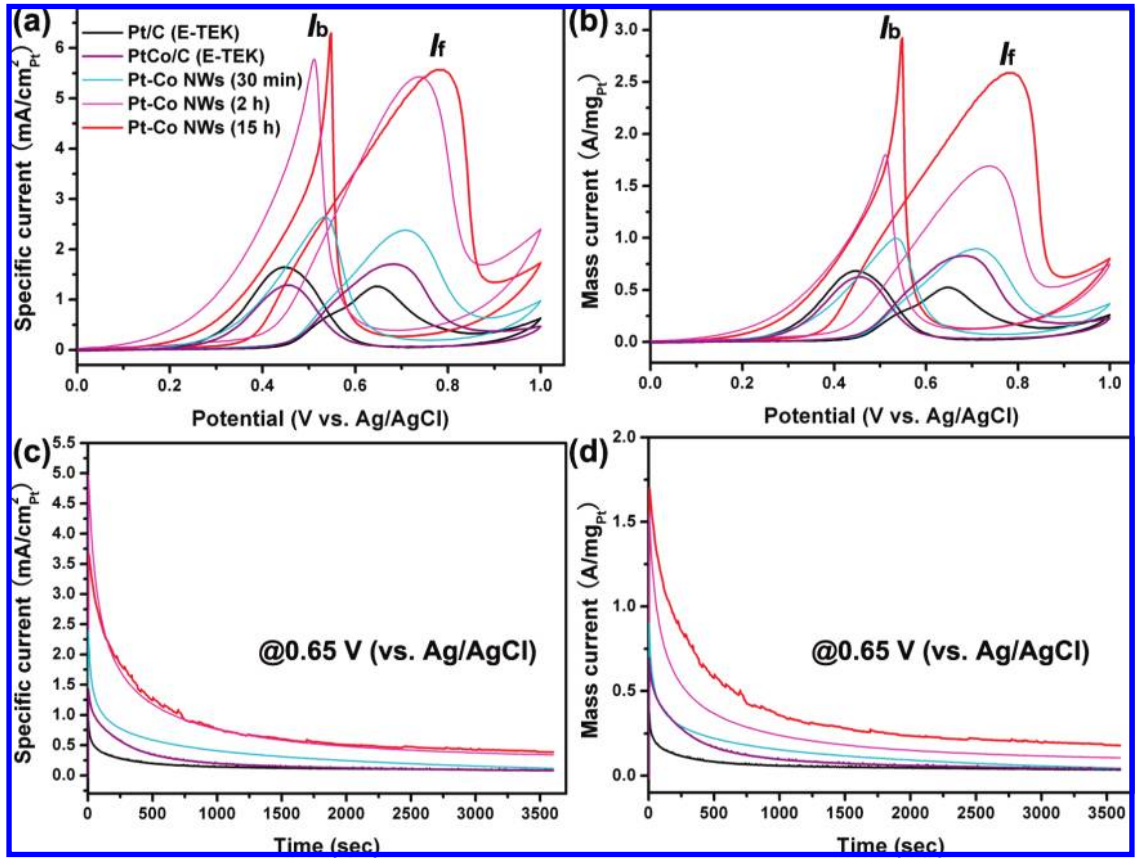

Figure 6. Electrocatalytic performance of the nanoporous Pt−Co alloy nanowires dealloyed for 30 min, 2 h, and 15 h toward methanol oxidation. (a,b) Cyclic voltammograms for methanol oxidation in 0.5 M H_2SO_4 and 1 M CH_3OH solution, which are normalized to the real Pt surface areas (specific activity) and the Pt mass (mass activity), respectively. Scan rate: 50 mV/s. (c,d) Pt real surface-normalized and Pt mass-normalized chronoamperograms (CAs) for methanol oxidation in 0.5 M H_2SO_4 and 1 M CH_3OH solution, which were recorded at 0.65 V (vs Ag/AgCl). For comparison, CVs and CAs of commercial Pt/C (30% Pt on Vulcan XC-72, E-TEK) and PtCo/C (30% PtCo (1:1 a/o) on Vulcan XC-72, E-TEK) catalysts are also included.

the nanoporous Pt_3Co nanowires replace the currently widely used Pt/C as anode catalysts, which may lead to the earlier commercialization of DMFCs.

The poisoning tolerance I_f/I_b, which is defined as the peak current ratio of the forward scan to backward scan (I_b), of the nanoporous Pt−Co alloy nanowire catalysts is also listed in Table 1. The I_f/I_b of Pt/C catalysts is 0.76, which is in good agreement with that reported by other authors.[3] It is found that the I_f/I_b of all nanoporous Pt−Co nanowire samples is higher than that of Pt/C, but lower than that of PtCo/C (1.32). The relatively small enhancement in I_f/I_b for the porous Pt−Co nanowires may be ascribed to the Pt-enriched feature of their outer surface, which is notwithstanding very favorable for methanol oxidation but less resistant to the poisoning of carbonaceous species.

In order to evaluate the long-term electrocatalytic performance, the chronoamperograms (i.e., current−time profiles) of the nanoporous Pt−Co nanowire catalysts were recorded with a bias at 0.65 V (vs Ag/AgCl) in 0.5 M H_2SO_4 and 1 M CH_3OH solution (Figure 6c,d). It is observed that the methanol oxidation current of Pt/C and PtCo/C catalysts decays with time and reaches an apparent steady state within 500 and 1250 s, respectively, while the current attenuation for the nanoporous Pt−Co nanowires takes a much longer time (>2000 s). Moreover, the steady state current of the nanoporous Pt−Co nanowires (30 min, 2 h, and 15 h dealloying samples) is found to be higher than that of Pt/C or PtCo/C, indicating a good performance. In addition, we also checked the morphology of the nanoporous Pt−Co nanowires after electrocatalytic measurements (Supporting Information, Figure S7). The nanoporous morphology can still be clearly seen even though the nanowires were subjected to several electrochemical cycling tests between 0 and 1 V (vs Ag/AgCl) and subsequent chronoamperometric measurement at 0.65 V (vs Ag/AgCl) for 1 h, which revealed a good structural stability.

As for the origin of the enhanced MOR catalytic activity of the nanoporous Pt−Co alloy nanowires, we assume that the following factors play a key role. First, it is known that the oxidation of methanol involves multistep adsorption and electron transfer, requiring multiple adjacent active Pt sites.[37] The unique features of high surface area and Pt-enriched outermost surface of the nanoporous Pt−Co nanowires meet this requirement well thus is favorable for the oxidation of methanol. Second, the Pt-enriched nature of the outer surface enables all surface sites of the nanoporous Pt−Co nanowires to be highly conductive. This is conducive to the reaction kinetics on the catalyst surfaces, and hence may result in an enhancement in activity.[21,31] Finally, the electronic and strain effects may play a major role in the activity enhancement.

It is known that alloying Pt with other metals can lower the electronic binding energy in Pt and promote the C−H cleavage reaction at low potential.[37] On the other hand, the strains, which widely exist in the dealloyed porous materials, have also been demonstrated to be favorable for the enhancement of electrocatalytic activity in Pt-based alloys.[42,43] On the basis of these arguments, it is not unexpected that the nanoporous Pt−Co alloy nanowires can exhibit distinctly enhanced catalytic performance toward methanol oxidation.

In summary, nanoporous Pt−Co alloy nanowires with different morphologies and controllable compositions were obtained by dealloying electrodeposited Pt_1Co_{99} nanowires in the presence of porous alumina templates in a mild acidic medium. Although using Pt−Co nanowire "precursors" with high Pt content as starting materials can also produce nanoporous Pt−Co alloy nanowires upon dealloying, the use of Pt_1Co_{99} nanowires for dealloying greatly extends the tunability in the composition of the resulting porous nanowires. We also demonstrated that the nanoporous Pt−Co alloy nanowires exhibit an enhanced electrocatalytic activity toward methanol oxidation (in comparison to state-of-the-art Pt/C catalysts) and therefore may potentially serve as efficient anode catalysts in direct methanol fuel cells.

Supporting Information Available: This material is available free of charge via the Internet at http://pubs.acs.org.

References

(1) Ding, Y.; Chen, M. W.; Erlebacher, J. *J. Am. Chem. Soc.* **2004**, *126*, 6876–6877.
(2) Ji, C. X.; Searson, P. C. *Appl. Phys. Lett.* **2002**, *81*, 4437–4439.
(3) Ge, X. B.; Wang, R. Y.; Liu, P. P.; Ding, Y. *Chem. Mater.* **2007**, *19*, 5827–5829.
(4) Xu, C. X.; Su, J. X.; Xu, X. H.; Liu, P. P.; Zhao, H. J.; Tian, F.; Ding, Y. *J. Am. Chem. Soc.* **2007**, *129*, 42–43.
(5) Yu, J. S.; Ding, Y.; Xu, C. X.; Inoue, A.; Sakurai, T.; Chen, M. W. *Chem. Mater.* **2008**, *20*, 4548–4550.
(6) Liu, H. T.; He, P.; Li, Z. Y.; Li, J. H. *Nanotechnology* **2006**, *17*, 2167–2173.
(7) Liu, Z.; Searson, P. C. *J. Phys. Chem. B* **2006**, *110*, 4318–4322.
(8) Qian, L. H.; Yan, X. Q.; Fujita, T.; Inoue, A.; Chen, M. W. *Appl. Phys. Lett.* **2007**, *90*, 153120.
(9) Lux, K. W.; Rodriguez, K. J. *Nano Lett.* **2006**, *6*, 288–295.
(10) Kramer, D.; Viswanath, R. N.; Weissmuller, J. *Nano Lett.* **2004**, *4*, 793–796.
(11) Biener, J.; Wittstock, A.; Zepeda-Ruiz, L. A.; Biener, M. M.; Zielasek, V.; Kramer, D.; Viswanath, R. N.; Weissmüller, J.; Baumer, M.; Hamza, A. V. *Nat. Mater.* **2009**, *8*, 47–51.
(12) Attard, G. S.; Bartlett, P. N.; Coleman, N. R. B.; Elliott, J. M.; Owen, J. R.; Wang, J. H. *Science* **1997**, *278*, 838–840.
(13) Yamauchi, Y.; Sugiyama, A.; Morimoto, R.; Takai, A.; Kuroda, K. *Angew. Chem., Int. Ed.* **2008**, *47*, 5371–5373.
(14) Peng, X. S.; Koczkur, K.; Nigro, S.; Chen, A. C. *Chem. Commun.* **2004**, 2872–2873.
(15) Koczkur, K.; Yi, Q. F.; Chen, A. C. *Adv. Mater.* **2007**, *19*, 2648.
(16) Yi, Q. F.; Chen, A. C.; Huang, W.; Zhang, J. J.; Liu, X. P.; Xu, G. R.; Zhou, Z. H. *Electrochem. Commun.* **2007**, *9*, 1513–1518.
(17) Erlebacher, J.; Aziz, M. J.; Karma, A.; Dimitrov, N.; Sieradzki, K. *Nature* **2001**, *410*, 450–453.
(18) Erlebacher, J.; Sieradzki, K. *Scr. Mater.* **2003**, *49*, 991–996.
(19) Erlebacher, J. *J. Electrochem. Soc.* **2004**, *151*, C614–C626.
(20) Parida, S.; Kramer, D.; Volkert, C. A.; Rosner, H.; Erlebacher, J.; Weissmuller, J. *Phys. Rev. Lett.* **2006**, *97*, 4.
(21) Snyder, J.; Asanithi, P.; Dalton, A. B.; Erlebacher, J. *Adv. Mater.* **2008**, *20*, 4883.
(22) Snyder, J.; Livi, K.; Erlebacher, J. *J. Electrochem. Soc.* **2008**, *155*, C464–C473.
(23) Pugh, D. V.; Dursun, A.; Corcoran, S. G. *J. Mater. Res.* **2003**, *18*, 216–221.
(24) Liu, L.; Lee, W.; Huang, Z.; Scholz, R.; Gösele, U. *Nanotechnology* **2008**, *19*, 335604.
(25) Yoo, S. H.; Park, S. *Adv. Mater.* **2007**, *19*, 1612.
(26) Shin, T. Y.; Yoo, S. H.; Park, S. *Chem. Mater.* **2008**, *20*, 5682–5686.
(27) Surendran, G.; Ramos, L.; Pansu, B.; Prouzet, E.; Beaunier, P.; Audonnet, F.; Remita, H. *Chem. Mater.* **2007**, *19*, 5045–5048.
(28) Wang, X. G.; Qi, Z.; Zhao, C. C.; Wang, W. M.; Zhang, Z. H. *J. Phys. Chem. C* **2009**, *113*, 13139.
(29) Park, K. W.; Choi, J. H.; Lee, S. A.; Pak, C.; Chang, H.; Sung, Y. E. *J. Catal.* **2004**, *224*, 236–242.
(30) Chen, L. Y.; Yu, J. S.; Fujita, T.; Chen, M. W. *Adv. Funct. Mater.* **2009**, *19*, 1221–1226.
(31) Xu, C. X.; Wang, L. Q.; Wang, R. Y.; Wang, K.; Zhang, Y.; Tian, F.; Ding, Y. *Adv. Mater.* **2009**, *21*, 2165.
(32) Ding, Y.; Kim, Y. J.; Erlebacher, J. *Adv. Mater.* **2004**, *16*, 1897.
(33) Sun, L.; Chien, C. L.; Searson, P. C. *Chem. Mater.* **2004**, *16*, 3125–3129.
(34) Sieradzki, K. *J. Electrochem. Soc.* **1993**, *140*, 2868–2872.
(35) Liu, Z. L.; Ling, X. Y.; Su, X. D.; Lee, J. Y. *J. Phys. Chem. B* **2004**, *108*, 8234–8240.
(36) Zhang, J. T.; Ma, H. Y.; Zhang, D. J.; Liu, P. P.; Tian, F.; Ding, Y. *Phys. Chem. Chem. Phys.* **2008**, *10*, 3250–3255.
(37) Antolini, E.; Salgado, J. R. C.; Gonzalez, E. R. *Appl. Catal., B* **2006**, *63*, 137–149.
(38) Lin, Z. H.; LIn, M. H.; Chang, H. T. *Chem.—Eur. J.* **2009**, *15*, 4656.
(39) Xu, D.; Liu, Z. P.; Yang, H. Z.; Liu, Q. S.; Zhang, J.; Fang, J. Y.; Zou, S. Z.; Sun, K. *Angew. Chem., Int. Ed.* **2009**, *48*, 4217–4221.
(40) Arunkumar, P.; Berchmans, S.; Yegnaraman, V. *J. Phys. Chem. C* **2009**, *113*, 8378.
(41) Tong, X. L.; Zhao, G. H.; LIu, M. C.; Cao, T. C.; Liu, L.; Li, P. Q. *J. Phys. Chem. C* **2009**, *113*, 13787.
(42) Koh, S.; Strasser, P. *J. Am. Chem. Soc.* **2007**, *129*, 12624.
(43) Mani, P.; Srivastava, R.; Strasser, P. *J. Phys. Chem. C* **2008**, *112*, 2770–2778.

NL902619Q